

Article

Microstructure and Fatigue Properties of Resistance Element Welded Joints of DP500 Steel and AW 5754 H22 Aluminum Alloy

Aleksija Đurić ¹, Dragan Milčić ^{2,*}, Zijah Burzić ³, Damjan Klobčar ⁴, Miodrag Milčić ², Biljana Marković ¹ and Vladislav Krstić ⁵

- ¹ Faculty of Mechanical Engineering, University of East Sarajevo, Vuka Karadžića 30, 71123 Sarajevo, Bosnia and Herzegovina; aleksija.djuric@ues.rs.ba (A.Đ.); biljana.markovic@ues.rs.ba (B.M.)
- ² Faculty of Mechanical Engineering, University of Niš, Aleksandra Medvedeva 14, 18000 Niš, Serbia; miodrag.milcic@masfak.ni.ac.rs
- ³ Military Technical Institute, Ratka Resanovića 1, 11030 Belgrade, Serbia; zijah.burzic@vti.rs
- ⁴ Faculty of Mechanical Engineering, University of Ljubljana, Aškerčeva cesta 6, 1000 Ljubljana, Slovenia; damjan.klobcar@fs.uni-lj.si
- ⁵ School of Engineering Management, University Union Nikola Tesla, Bulevar vojvode Mišića 43, 11000 Belgrade, Serbia; vladislav.krstic@fim.rs
- * Correspondence: dragan.milcic@masfak.ni.ac.rs

Abstract: The modern concept of lightweight design (LW) requires the application of different materials in one structure (multi-material structures). The structure of different materials has a good perspective for application in the automotive and aerospace industries but only if it is possible to achieve a quality joint between different materials. The most used technology for joining different materials in the automotive industry is Resistance spot welding (RSW). Due to different mechanical, physical, and chemical properties, the joining of different materials by RSW technology does not provide a quality joint, and accordingly, alternative technologies for joining different materials have emerged. Resistance element welding (REW) was developed to enable joint of different materials. This paper presents the welding of AW 5754 H22 Al alloy (1.0 mm-thick) and DP500 steel (1.5 mm-thick) using novel REW. The peak load, absorption energy, microstructure, microhardness and fatigue strength of the REW joint has been investigated. The joint of the same materials has been done also using conventional RSW to compare some results. The results that will be presented in this paper show that that REW can achieve reliable joining of the two materials at relatively low welding currents compared to RSW. Using REW process with a significantly lower welding current, satisfactory mechanical characteristics of the weld joint can be achieved, so peak load is between 2300–2500 N, displacement is between 2.5–3 mm and the absorption energy is between 3.3–5.7 J. REW joints showed fatigue strength with the fatigue limit of 882 N.

Keywords: resistance spot welding; resistance element welding; dissimilar materials joints; microstructure; microhardness; fatigue strength



Citation: Đurić, A.; Milčić, D.; Burzić, Z.; Klobčar, D.; Milčić, M.; Marković, B.; Krstić, V. Microstructure and Fatigue Properties of Resistance Element Welded Joints of DP500 Steel and AW 5754 H22 Aluminum Alloy. *Crystals* **2022**, *12*, 258. <https://doi.org/10.3390/cryst12020258>

Academic Editor: Shanping Lu

Received: 1 January 2022

Accepted: 2 February 2022

Published: 14 February 2022

Publisher's Note: MDPI stays neutral with regard to jurisdictional claims in published maps and institutional affiliations.



Copyright: © 2022 by the authors. Licensee MDPI, Basel, Switzerland. This article is an open access article distributed under the terms and conditions of the Creative Commons Attribution (CC BY) license (<https://creativecommons.org/licenses/by/4.0/>).

1. Introduction

In recent years, car manufacturers increasingly have to meet the requirements related to environmental protection, i.e., they should minimize the damage that the use of cars leaves on the environment, starting from production until their dismantling. New European regulations on CO₂ emissions—95 g/km CO₂ in 2020 and a target of 30% further reduction by 2030—have been changing the game as they are now coupled with a financial penalty [1]. Since weight lightening strongly impacts fuel consumption, 10% weight reduction leads to a fuel economy of 5.5% and so CO₂ emission [2], the use of a lightweight (LW) design is now necessary.

The modern concept of LW design requires the application of different materials in one structure (multi-material structures). The combination of different materials, such as high strength steel, magnesium alloys, aluminum alloys and fiber reinforced composites can be used to improve components in terms of various requirements (component properties, manufacturability, costs, etc.). With the reduction of component weight, low costs and feasibility in mass production, multi-material design approaches are the ideal compromise for the mass automotive lightweight construction of the future [3]. A prerequisite for achieving multi-material structures is the application of efficient and cheap technologies for joining different materials. The structure of different materials has a good perspective for application in the automotive and aerospace industries but only if it is possible to achieve a quality joint between different materials.

The most used technology for joining different materials in automotive industry is Resistance spot welding (RSW). Due to different mechanical, physical and chemical properties, the joining of different materials by RSW technology does not provide a quality joint, and accordingly, alternative technologies for joining different materials have emerged. Resistance element welding (REW) was developed to enable joint of different materials. This technology does not require significant modification of existing equipment in factory, which is its great advantage. REW is an innovative thermal-mechanical joining technology and it is a mature joining process, proved by the first series of applications [4]. In comparison to mechanical joining technology and adhesive joining, REW has better characteristics in terms of the possibility of joining ultra-high strength steel and other lightweight metals and also in terms of joint strength and reliability [5].

This paper presents the investigation of microstructure and mechanical properties (peak load, absorption energy, microhardness and fatigue strength) of REW of DP500 steel and aluminum alloy AW-5754 H22 sheets. These two materials were selected as adequate representatives of multi-material structures, which are primarily applied in the automotive industry. DP steels belong to the Advanced High Strength Steel (AHSS) that are mainly composed of dispersed islands of martensite in a ferrite matrix. The ductility is controlled by the ferrite, while the strength is controlled by the martensite [6]. The DP500 has good forming and welding ability, and is very suitable for the manufacture of safety parts in cars such as reinforcement elements [7]. The DP500 steel is very suitable for RSW, and with optimized welding parameters, very good mechanical characteristics of the joint can be obtained [8]. Recently, several groups of aluminum alloys have been used in the automotive industry, the most common of which are alloys AA5754 and AA6082. The alloy AA5754 is of medium strength when compared to other aluminum alloys and is mostly used for sports car bodies [9]. The joint of the same materials has been done also using conventional RSW to compare some results. Failure mode during the tensile-shear test is a conservative measure for quality control of the spot welds. Moreover, the paper presents the determination of failure mode type during static and dynamic tensile-shear tests with fracture surface morphology.

2. State of Art in the Field of Resistance Spot Welding (RSW) and Resistance Element Welding (REW) of Aluminum and Steel Sheets

RSW of aluminum and steel alloy encounters many problems, primarily due to differences in thermal, mechanical and physical properties, and due to the appearance of brittle Fe-Al intermetallic compound (IMC). Significant research has been done on the control of the IMC interlayer during the RSW process and due to good metallurgical compatibility with both materials, it has been concluded that zinc (Zn) or magnesium (Mg) coating on steel can improve the load-capacity of aluminum/steel joint [10–12]. The quality of the RSW welding process is also affected by the presence of an oxide layer (Al_2O_3) on the aluminum site, so before welding, it is necessary to remove that oxide film and that makes the process yet more difficult and expensive [13].

One of the quality parameters of the RSW joint is the fracture mechanism or failure modes during the tensile-shear test. Generally, RSW failure occurs in two modes: interfacial

(IF) and pullout (PF). Fracture modes that can be identified for Al/steel RSW are two types of interfacial fracture (interfacial failure via crack propagation through IMC layer and interfacial failure (IF) via rupture mainly between the intermetallic phases and the Al base material) and pullout fracture. Pullout fracture is the most acceptable or only acceptable mode for the automotive industry. It is not easy to achieve PF mode with RSW joining aluminum alloy and steel but it is of note that obtaining PF mode leads due to severe Al sheet thinning. Obtaining a pullout fracture is possible by reducing the thickness of the IMC layer, and this can be achieved by increasing the welding current which leads to a decrease in the thickness of the aluminum in the nugget and that leads to reduction of capacity of the joint [14,15].

Studies about fatigue behavior of the RSW joint of aluminum alloy and DP steel are very limited, with most studies usually based on the analysis of the alloy of RSW joining aluminum alloy and other steel (non-DP steels) [16–18], then the fatigue analysis of RSW joint of DP steels and other steels [19,20] or two DP steels [21,22].

Shi et al. [23] investigated RSW dissimilar joint of aluminum-steel produced using a multi-ring domed (MRD) electrode and multi-solidification weld schedules with aluminum in both the positive and negative polarity conditions. One conclusion was that increasing notch root angle produced a slight increase in static tensile peak load, it also improved fracture modes and was beneficial for increasing fatigue life because the principal strain decreased with increasing notch root angle.

REW is developed as an alternative to the resistance spot welding for joining dissimilar materials especially in the automotive and aerospace industry. The complete REW process is shown in Figure 1. REW is a process that begins with the insertion of steel, called an element, into aluminum, magnesium, or other lightweight material. After the element is inserted into the lightweight material, the procedure of classic resistance spot welding is followed. One of the first applications of the REW process in high-volume production was at manufacturing the parcel shelf for the VW's Passat B8 limousine, saving over a kilogram in weight in this component alone [24].

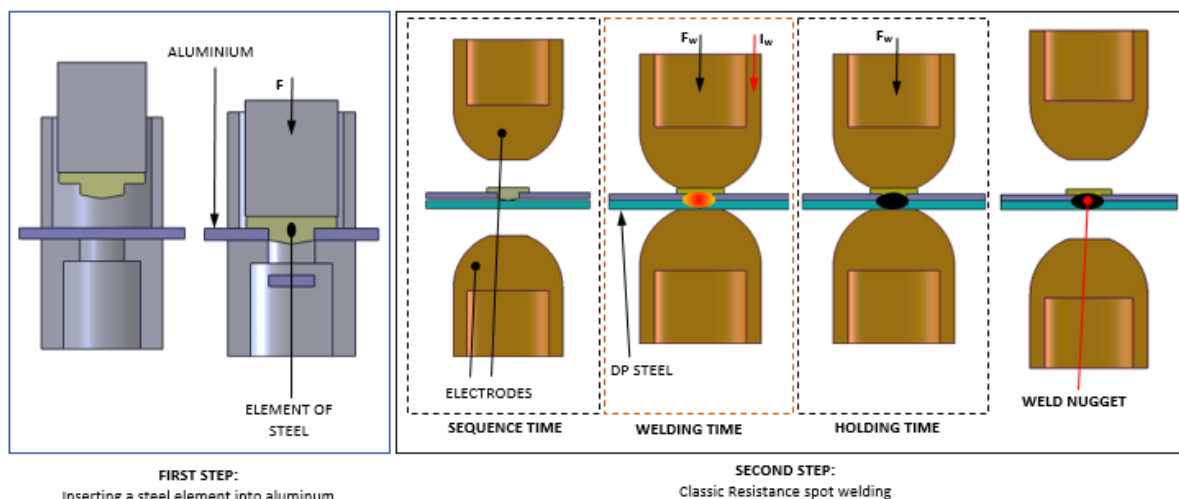


Figure 1. Process of Resistance element welding (F —pressure force, I_w —welding current, F_w —Electrode force).

An additional element in the REW process is also called rivet, so this process can also be called resistance spot welding with rivets. Studies about REW are also very limited, there are some scientific and technical papers that compared RSW and REW joining of steel and aluminum alloy.

Zhanxiang Ling et al. [25] analyzed the mechanical properties, nugget forming method and microstructure of resistance element welding with AHSS 22MnMoB steel and aluminum alloy 6061. This paper compares this procedure with conventional RSW, and concluded

that RSW is barely capable of joining Al 6061 alloys and 22MnMoB steel, while REW can achieve reliable joining of the two materials at relatively low welding currents. The paper also shows that the maximum load of the REW joint is up to seven times greater than the maximum load of the RSW joint, while the maximum energy absorbed at the REW joint is up to 100 times greater than the same energy at the RSW joint. RSW joint was done with a welding current of 12–20 kA with an interval of 2 kA and the REW joint was done with a welding current of 6–10 kA with an interval of 1 kA. The nugget structure consists mainly of martensite, and the structure of the heat-affected zone depends on the distance from the center of nugget. Different structures correspond to different microhardnesses. An IMC layer is formed between the element and the aluminum, and the layer consists of FeAl, Fe₂Al₅ and FeAl₃.

Zhanxiang Ling et al. [26] in a paper published in 2017 compared the mechanical properties of RSW and REW joints of aluminum alloy 6061-T6 and DP780 steel depending on the welding current. The RSW joint was done with a welding current of 12–16 kA with an interval of 1 kA and the REW joint was done with a welding current of 6–10 kA with an interval of 1 kA. The element used for the REW joint was made from Q235 steel. Results in the paper showed that REW joints have higher static and fatigue strength than RSW joints. Generally, based on previously presented studies, it can be concluded that the REW technology is more suitable for application than the RSW for joining steel and aluminum alloy sheets. Joints with good mechanical characteristics can be achieved with a relatively low welding current.

Ranfeng Qiu et al. [27] have also shown in their paper that the REW process is a more efficient method for joining mild steel and aluminum alloy 6061 than the conventional RSW procedure. In addition, the authors have shown that between the element and the aluminum form a compound FeAl, while between the steel and aluminum form a compound FeAl₃.

In their research, Heidrich D et al. [28] compared the fatigue strength of joints obtained by Resistance rivet spot welding (RRSW), which is very similar to REW and self-piercing riveting (SPR). For this purpose, steel material of CR340 with 0.8 mm-thick and aluminum alloy with Al 6016 with 1.0 mm-thick were selected, as well as a combination of the same materials but with 1.5 mm-thick steel. The rivet used for this experiment was 6.5 mm-thick and 5.6 mm in nominal diameter made of S355 steel. The fatigue test was performed with force ratio $R = 0$ for four different types of specimens: (a) flat specimen with one joint and 50 mm overlap tested with a frequency of 10 Hz, (b) flat specimen with two joints and overlap of 50 mm, also tested with a frequency of 10 Hz, (c) H-specimen with 10 spots shear loaded, tested with a frequency in the range of 83 to 95 Hz and (d) H-specimen with 10 points peeling loads and tested with a frequency in the range of 34 up to 38 Hz. A study by these authors showed that RRSW has better static and dynamic characteristics than SPR for a steel sheet thickness of 1.5 mm, while this is not the case for a joint where the steel sheet thickness was 0.8 mm. The RRSW joining can also be done without inserting a rivet in the aluminum alloy before welding. Sizhe Niu et al. [29] presented that the maximum lap shear strength of the RRSW joints of aluminum alloy 6061 and press hardened steel could get up to 481.4 MPa at the parameters: welding current 8 kA and welding time 200 ms.

This joining technology is also suitable for joining thermoplastic materials and metals, primarily steel [30]. Furthermore, there are some studies on REW joining of steel and magnesium alloys. S.M. Manladana et al. [31] in their paper concluded that conventional RSW is not suitable for joining Mg alloy / ASSs in multi-sheet configurations, but REW has the potentials of being a reliable technique for joining Mg alloy and ASS sheets in three-sheet configurations. In the paper of the author S.M. Manladan et al. [32], the microstructures and mechanical properties of joints of dissimilar materials were investigated. AZ31 Mg alloy 1.5 mm-thick and 0.7 mm-thick 316L ASS steel was bound by the REW process, Q235 steel was used as an element. This paper also shows that the mechanical properties of REW joints are superior to traditional RSW joints and that the failure mode of REW joints changes from IF to PF mode with the increasing of the welding current.

3. Experimental Procedure

For this research 1 mm-thick aluminum alloy AW 5754 H22 Al and 1.5 mm-thick DP500 steel were used. Q235 steel rivet was used as the auxiliary element. The chemical compositions and basic mechanical properties of these materials are shown in Table 1.

Table 1. Mechanical proprieties and chemical composition of materials used in this research.

Material	Chemical Composition (%)										
	C	Cr	Si	Mn	P	Fe	S	Mg	Al	Cu	
DP 500	0.1	/	0.5	1	0.025	Bal.	0.01	/	0.015	/	
AW 5754	/	0.3	0.4	0.4	/	0.3	/	3.6	Bal.	0.1	
Q235	0.29	/	0.28	1.03	0.04	Bal.	0.05	/	/	0.2	
Mechanical properties											
	Yield strength $R_{p0,2}$ (MPa)			Tensile strength R_m (MPa)				Elongation A_{80} (min %)			
DP 500	330			550				20			
AW 5754	185			245				15			
Q235	250			475				20			

The welding specimens were 30 mm × 100 mm for REW joining (Figure 2a). The element with 4 mm diameter was inserted into the aluminum with force pressure of 300 N. The welding specimens were 30 mm × 105 mm for RSW joining (Figure 2b). Before welding, industrial alcohol was used to clean the specimens. Classic RSW welding for both cases were done using RSW machine manufactured by Kocevar & Sinovi (Polzela, Slovenia), which is managed using the BOSCH 6000 software (Bosch, Stuttgart, Germany). Welding was carried out using electrode type F1.

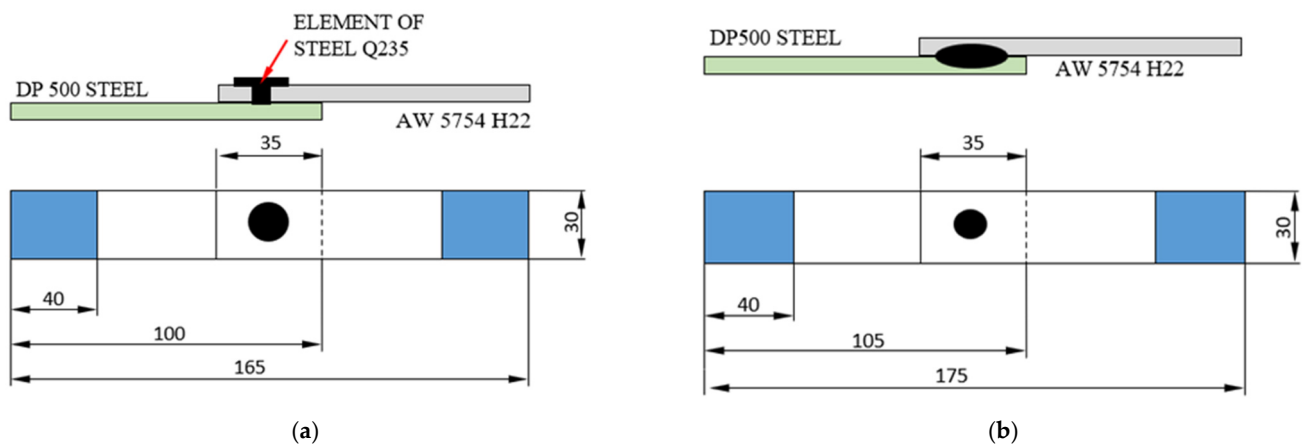


Figure 2. Dimensions of specimens: (a) Resistance element welding; (b) Resistance spot welding.

In order to compare the peak load and absorption energy, a tensile-shear static test was performed for specimens welded with RSW and REW technology with the welding parameters shown in Table 2. Weld current I was selected for experimentation on three levels. Electrode force F and weld time T were constant. Other welding parameters are: squeeze time (SQZ = 300 ms), hold time (HLD = 300 ms), pre-heating time (Pre-Weld = 0 ms), Cool Time (CT = 0 ms), Up Slope Time (UST = 0 ms), and Down Slope Time (DST = 0 ms) which were also constant during the experiment for both cases of welding.

Table 2. Welding parameters layout for tensile-shear static test.

Run	Mark	Weld Current I (kA)	Electrode Force F (kN)	Welding Time T (ms)
1	K-1	9.5		
2	K-2	12.5	3.68	280
3	K-3	16.5		
4	REW-1	6		
5	REW-2	8	3.68	60
6	REW-3	10		

The tensile-shear tests were performed according to standard ISO 14273:2016 at a cross-head speed of 2 mm/min with a Beta 50-7/6×14 testing machine. These tests were done with three replicates. The failure energy was calculated by measuring the area under the load-displacement curve up to the maximum load point. Failure energy (W_{max}) represents the energy absorption capability of the welds before failure initiation [19] and this energy is most important by a car crash. Metallographic samples were cut from the center of the joints. The samples were ground and polished based on standard metallography procedures. The Q235 and DP500 steel side were etched using 4% nital solution (7 s) and the Al side was etched using H₂O and HF solution (25 s). Microstructures of joints were observed with a Keyence VHX-6000 microscope (Keyence, Osaka, Japan).

The fatigue and microhardness test were done only for REW joint welded with the following parameters: welding current of 10 kA, electrode force of 3.68 kN and welding time of 60 ms. Vickers micro-hardness tester Zwick/Roell ZHU 2.5 was used to measure the microhardness variations cross the joint under the load of 5 N for 12 s. The microhardness test was performed on a cross-section in the direction of three vertical lines through all characteristic zones of the joint as shown in Figure 3.

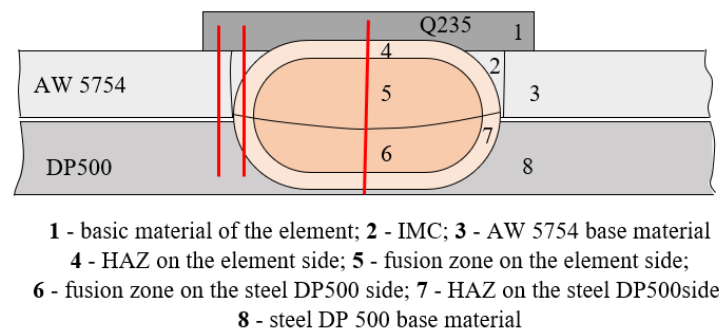


Figure 3. Schematic representation of characteristic zones and the line along which the microhardness measurement was made for REW joint.

The tension-shear fatigue test of REW joints was conducted on a Shimadzu Servopulser E100kN machine, with the sinusoidal waveform in load-control mode at a force ratio of $R = 0.1$ and frequency of 30 Hz.

4. Results and Discussion

4.1. Resistance Spot Welding

Tensile-shear load-displacement curves of Al/steel RSW joint for three specimens (K-1, K-2, K-3) are shown in Figure 4. Peak load is between 1200–2500 N and displacement is between 0.5–1.1 mm. Furthermore, for these three specimens, the failure energy or absorption energy is 0.29, 1.18, and 1.72 J respectively. The line is not straight (the magnified region of the curve) due to the cracking brittle IMC interlayer. The experimental results showed that the welding current has significantly affected the load-displacement characteristics of these welded joints. Maximum failure load (around 2500 kN) and energy (around 1.7 J) were determinate with a welding current of 16.5 kA.

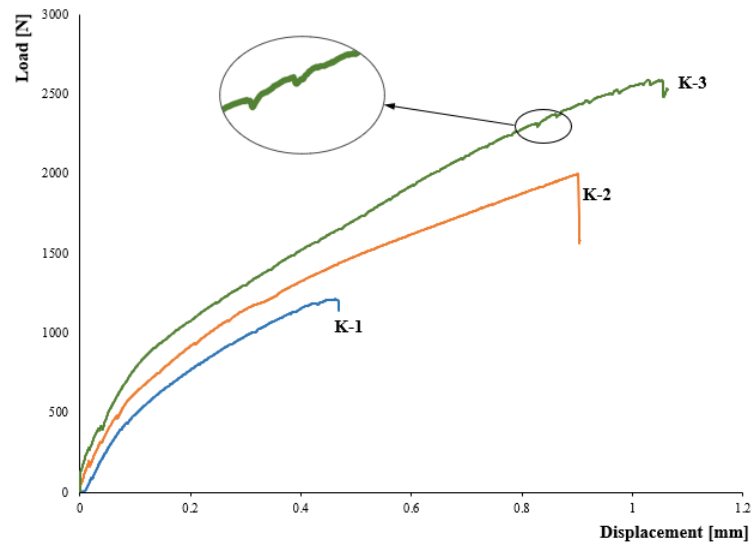


Figure 4. Tensile-shear load-displacement curves of Al/steel RSW joint.

Determination of failure mode of RSW joint during the tensile-shear test is very important because RSWs failed in pullout mode (acceptable case) during the tensile-shear test are expected to fail in pullout mode during cross-tension, peel and chisel tests [33]. Fracture surface morphology for all RSW specimens are shown in Figure 5a. Some Al splash was found around the welded area and also the small bonded or weld area was found which is the reason for the lower tensile shear strength of the lap joint. When the joint is made with a welding current of 12.5 or 16.5 kA (specimens K2 and K3), spot welds were failed by one-sided pullout failure mode. Thus, by increasing the welding current, the tensile strength and failure energy of the joint is also increased, and it is possible to obtain a joint that bursts in a one-sided PF module.

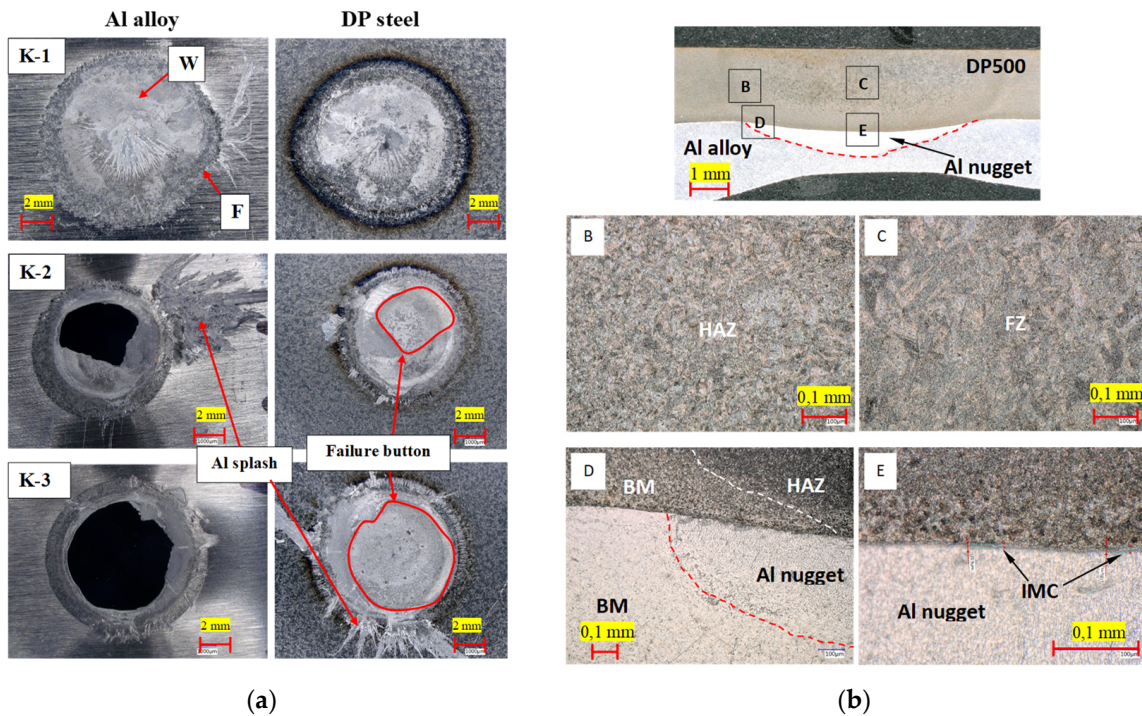


Figure 5. (a) Fracture surface morphology (W—welding area, F—fracture location); (b) Microstructure of AW5754/DP 500 steel RSW joint.

It has already been pointed out that an increase in the welding current at a steel-aluminum joint can lead to a decrease in the thickness of the aluminum in the nugget but also to significant damage to the electrode and a reduction in its service life. The reduction of the electrode life is significantly affected by the oxide layer on the aluminum side, the damaged electrode further affects the quality of the joint [34].

Figure 5b shows the typical microstructure of AW5754/DP 500 steel RSW joint.

Region B (Figure 5b) shows Heat Affected Zone (HAZ) of DP 500. As is known, HAZ is a recrystallization zone. Insufficient heat input helps to produce fine martensite in HAZ. The fusion zone (FZ) of DP 600 is martensite and this is shown in Region C. Region D shows the line between the base material and HAZ. The IMC is shown in Region E.

4.2. Resistance Element Welding

4.2.1. Tensile-Shear Static Test

Figure 6a shows typical tensile-shear load-displacement curves of Al/steel REW joint for three specimens (REW-1, REW-2, REW-3). Peak load is between 2300–2500 N, displacement is between 2.5–3 mm and the absorption energy is between 3.3–5.7 J. The experimental results showed that the welding current in range from 6 kA to 10 kA has not big significantly affected the load-displacement characteristics of these welded joints.

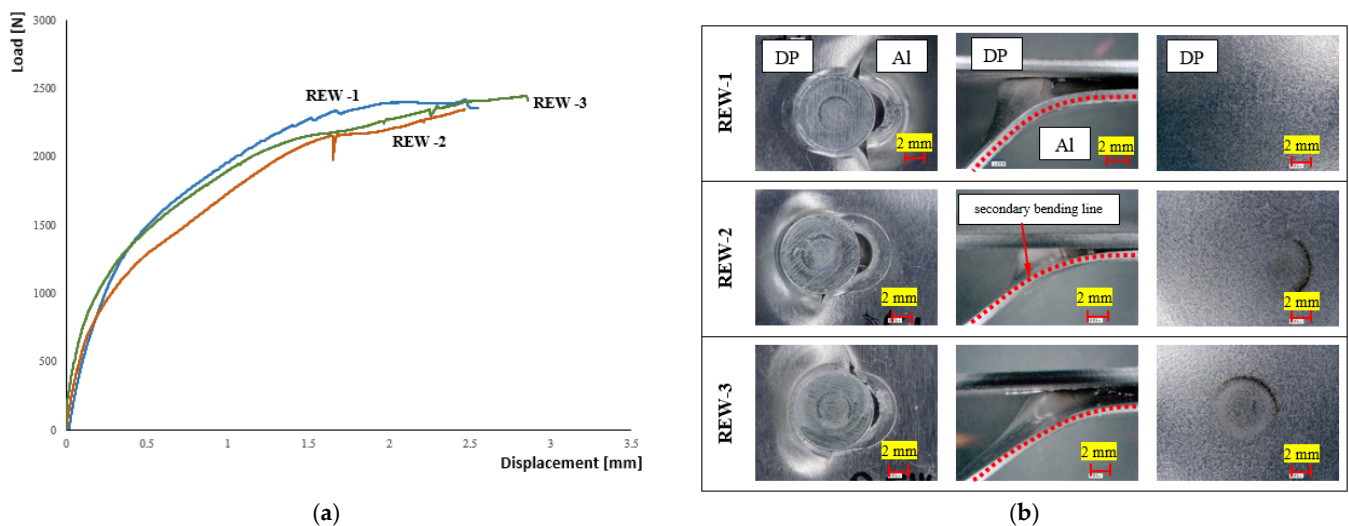


Figure 6. (a) Tensile-shear load-displacement curves of Al/steel REW joint; (b) Fracture surface morphology of Al/steel REW joint.

All REW specimens fail in PF mode and fracture surface morphology for all REW specimens is shown in Figure 6b. This PF type of failure mode is also observed in riveted and bolted joints, and it is also referred to as tension failure (TF).

Since the PF (TF) sustained higher load and is more complex, it is characterized further. During lap-shear tests, due to the eccentricities in the load path, out-of-plane deformations referred to as secondary bending occur [31]. As shown in Figure 6b, the Al alloy sheet experienced secondary bending. A compressed region occurred on the primary bearing surface of the Al alloy under the rivet. The size of this region increased as the test progressed. As the severity of the secondary bending increased, due to the reduction in stiffness and limited ductility of the Al alloy, failure occurred abruptly through the hole center. There was no secondary bending on the DP steel side, primarily due to the higher load capacity of the DP steel compared to the Al alloy.

4.2.2. Microstructure and Microhardness

The typical macrostructure of the REW joint of steel DP500 and aluminum alloy AW5754 H22 is shown in Figure 7. The larger part of the nugget is in the Q235 steel rivet for all combination. This formation of the asymmetrical nuggets can be attributed to the differences in electrical resistivity and thermal conductivity. The welded joint can be divided into three parts: fusion zone (FZ), heat affected zone (HAZ) and base metal (BM).

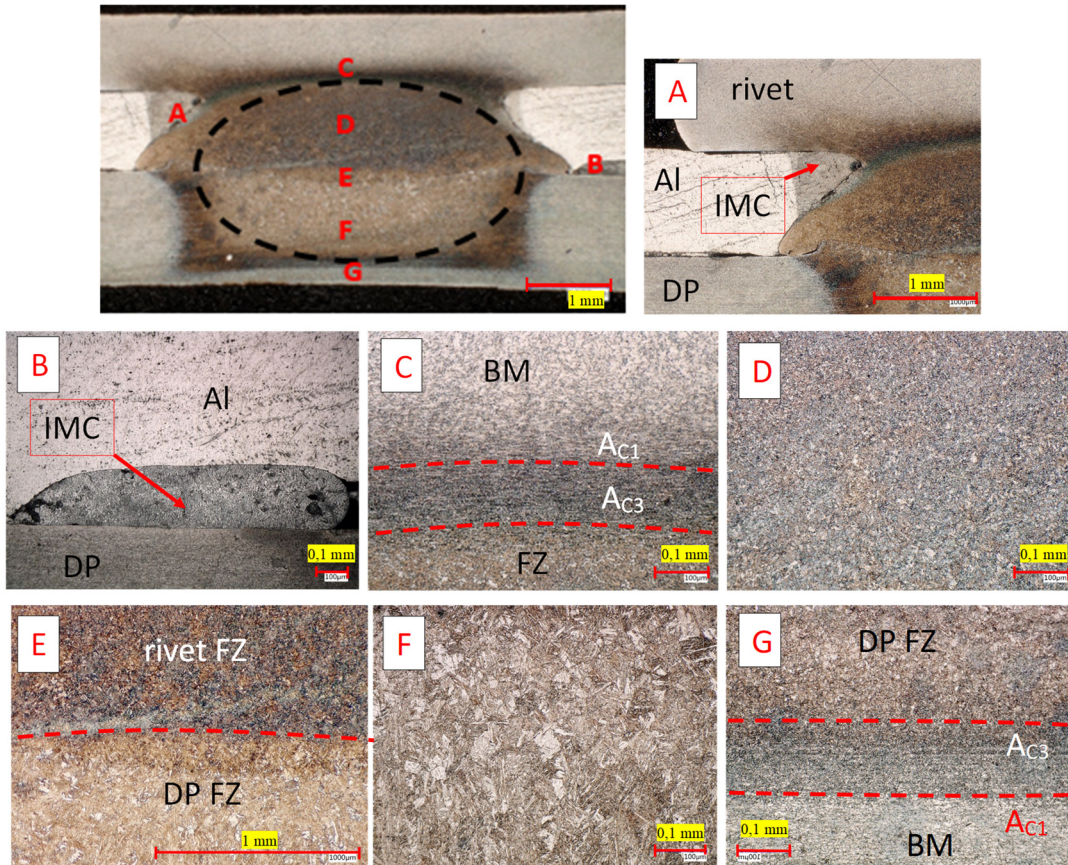


Figure 7. Microstructure of AW5754/DP 500 steel REW joint welded with 10 kA current.

RSW was implemented first on the rivet which leads to the fusion of the rivet (element) and then on the aluminum alloy near the rivet/Al interface. The diffused material between rivet and aluminum alloy is subsequently solidified and generates FeAl from a-Fe (Region A). Region B also shows the appearance of an intermetallic compound (IMC) but now between DP steel and aluminum alloy.

Region C shows the microstructures in the heat-affected zone (HAZ) of rivet Q235. This HAZ can be divided into two different zones: inter-critical HAZ and upper-critical HAZ. The maximum temperature that is attained in this zone is above A_{c3} (upper-critical HAZ), and the BM completely transforms into austenite. As a result of the fast cooling, the austenite transforms into martensite. The peak temperature reached in this zone is between A_{c1} and A_{c3} (inter-critical HAZ, and the BM microstructure transformed into a mixture of ferrite and austenite. After cooling, the austenite transformed into pearlite while the ferrite is retained. The BM microstructure also consisted of ferrite and pearlite, but the volume fraction of the pearlite is less than that of the inter-critical HAZ. The D show fusion zone (FZ) region at the rivet site and Region E show the interface between the DP steel and the rivet.

Peak temperature in the FZ surpasses the liquidus temperature. FZ on DP site exhibits a complex microstructure including columnar grains of martensite, upper bainite, allotriomorphic ferrite and Widmanstaatten ferrite, which is also the result of research of

authors Ling, Z et al. [26]. The martensite formation in the FZ in DP steel is attributed to the inherently high cooling rate of the resistance spot welding process due to the presence of water-cooled copper electrodes and their quenching effect as well as the short welding cycle (Region F).

HAZ on DP site can be divided into four subregions: the subcritical, inter-critical, fine grained and coarse-grained heat-affected zones (Region G). In the subcritical HAZ, the peak temperature is below Ac1 resulting in the tempering of martensite. The peak temperature of the inter-critical HAZ ranges between Ac1 and Ac3. Increasing peak temperature results in an increase of austenite, which transforms into martensite due to the rapid cooling rate. Peak temperature exceeds Ac3 in the fine grained HAZ and holds a short time, and grains have little time to grow further. Peak temperature in the coarse-grained HAZ is well above Ac3 and has extended time to coarsen the austenite grains compared to the fine grained HAZ.

The vertical microhardness profiles of REW joint is shown in Figure 8.

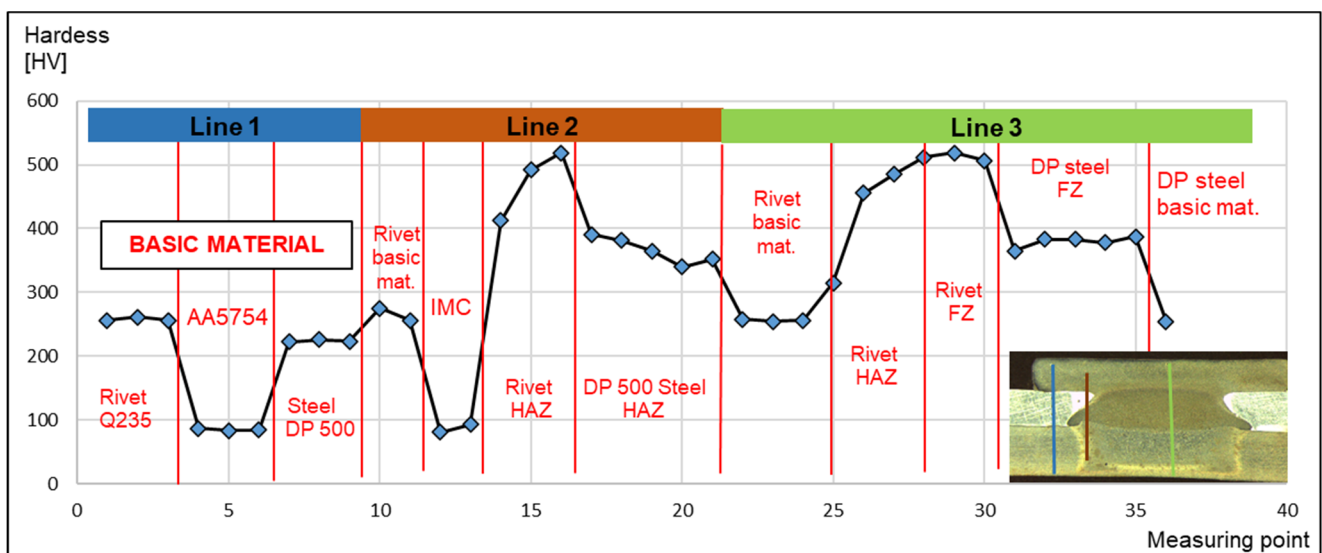


Figure 8. Vertical microhardness profiles of AW5754/DP 500 steel REW joint welded with 10 kA current.

As shown in Figure 8, the microhardness of the fusion zone in DP steel is on average 379 HV. The average hardness of the DP steel base material is 223 HV. The formation of bainite and martensite in the FZ explains the higher hardness of the FZ compared to the BM hardness [35]. The HAZ in Q235 steel rivet exhibited the highest hardness (more than 500 HV), which is due to the martensitic microstructure. It is also noted that the hardness of the rivet fusion zone is very high, about 500 HV. The hardness of IMC is similar to the hardness of Al alloy basic material, approximately 85 HV. Such a high value of the fusion zone microhardness allows failure in PF mode. Aluminum has the lowest hardness and strength in this joint, so it is obvious that the joint fails through aluminum, primarily around the weld because it is weakened there with a hole that served to insert the element.

According to the presented results and previous research [25,26] can be expected that the nugget of REW joint steel and aluminum alloy will be asymmetric and the fusion zone will consist mainly of martensite. The martensite formed in the fusion zone allows high hardness of weld, PF failure mode, and good strength of joint.

4.2.3. Fatigue Tensile-Shear Test

The dependence of the maximum tensile-shear load on the number of cycles to failure (S-N curve) for REW joint welded with 10 kA current is shown in Figure 9. Defined as the runout load at 10×10^6 cycles, a fatigue limit of 882 N was obtained for the REW of DP500 steel and aluminum alloy AW5754.

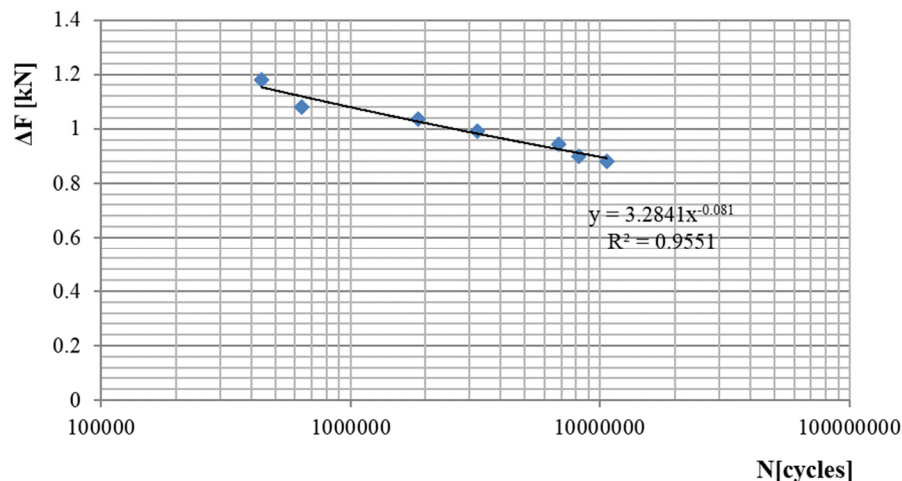


Figure 9. Dependence of the maximum tensile-shear load on the number of cycles to failure for REW joint welded with 10 kA.

In all specimens (from 2-2 to 2-7) there was a fracture through the aluminum alloy at the joint, very similar to the static test, so it can be considered a PF failure mode (Figure 10). The initial crack was formed below the element in an aluminum alloy, which grew with an increasing number of cycles, and eventually caused the specimens to break. This type of cracking at fatigue testing can be explained by the fact that the fusion zone consists primarily of the very high hardness of martensite, but the aluminum is very soft and weakened by the IMC layer in the vicinity of the weld. So, since the fatigue cracks in Al sheet metal touched the weld spot, it could have been caused by the hardness reductions around the weld spot [28].



Figure 10. REW specimen fracture after dynamic tensile-shear testing.

4.3. Comparison of RSW and REW

Figure 11 shows a comparison of peak load and failure energy value for RSW and REW joint of A5754 aluminum alloy and DP500 steel sheets. This experiment shows that with the significantly lower welding current in the REW process, satisfactory mechanical characteristics of the weld joint can be achieved. With a welding current of 6 kA (REW1) in the REW joint, approximately the same values of the peak load are obtained as in the RSW joint welded with a welding current of 12.5 kA (K2) and almost double higher failure energy. When welding with a current of 10 kA (REW3) in a REW joint, a slightly higher value of the peak load is obtained in relation to a joint welded with a welding current of 16.5 kA (K3), and the absorbed energy in a REW joint is up to three times higher than in an RSW joint. The higher energy absorbed by the REW joint is due to the cracking joint through the base material of aluminum. The advantage of the REW connection is not only reflected in the higher failure energy, i.e., energy absorption but also in the fact that it joins steel to steel, thus extending the life of the electrode. It has already been pointed out that an increase in the welding current at a steel-aluminum joint can increase the load capacity of the joint but also to significant damage to the electrode and a reduction in its service life.

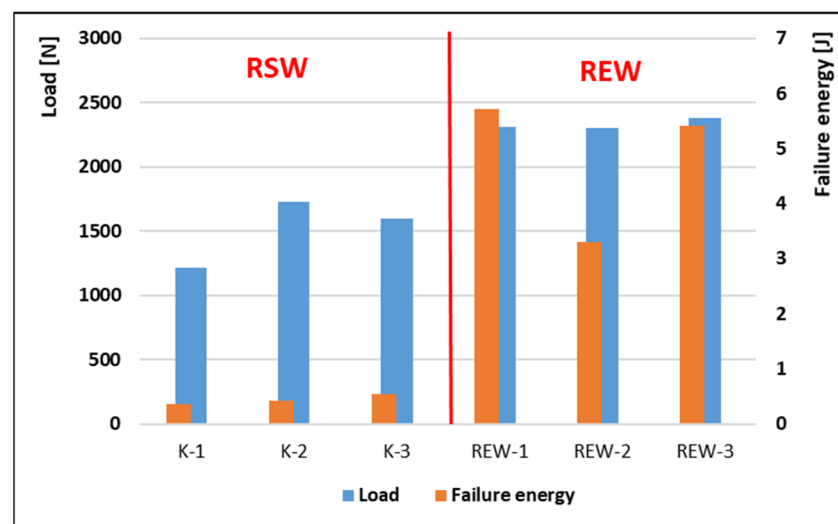


Figure 11. Comparison of peak load and energy absorption of RSW and REW joints.

The comparison was made on the basis of welding current, as a parameter that has the greatest impact on the mechanical properties of RSW and REW joints, so REW can achieve reliable joining of the DP steel and aluminum alloy at relatively low welding currents compared to RSW, which are also the conclusions of most previously published studies [25–27].

5. Conclusions

This paper presents the welding of AW 5754 H22 Al alloy (1.0 mm-thick) and DP500 steel (1.5 mm-thick) using novel Resistance element welding (REW). The peak load, absorption energy, microstructure, microhardness and fatigue strength of REW joint were obtained. The joint of the same materials was done using conventional Resistance spot welding (RSW) to compare results. The main findings of this paper can be summarized as follows:

1. REW is a more effective method than the conventional method for joining steel and aluminum alloy. With usage of REW process with the significantly lower welding current, satisfactory mechanical characteristics of the weld joint can be achieved. Moreover, the maximum absorption energy of RWE was 5.72 J, which is over 3.5 times higher than the RSW. All REW specimens fail in PF (TF) mode with experienced secondary bending of Al alloy sheet. By usage of RSW joining, specimens welded

- with current 9.5 kA fail in IF mode and other specimens (12.5 kA and 16.5 kA) fail in one-side PF mode.
2. A nugget of the REW was formed first at the interface of the rivet and DP steel. The larger part of the nugget is in the Q235 steel rivet. This formation of the asymmetrical nuggets can be attributed to the differences in electrical resistivity and thermal conductivity. The nugget of the resistance element weld joint consists mainly of martensite, and the heat-affected zone structure varies according to the distance from the nugget. An IMC layer was formed between the rivet and aluminum and also between aluminum and steel. Different microstructures correspond to different microhardnesses. The microhardness of the rivet fusion zone ranged from 460 to 500 HV, while the microhardness of the fusion zone in DP steel ranged from 360 to 380 HV. The HAZ in Q235 steel rivet exhibited the highest microhardness (more than 500 HV). The microstructure of the RSW joint shows that the fusion zone (FZ) of the DP steel site is composed of martensite³. REW joints of these two materials showed fatigue strength with the fatigue limit of 882 N at $10 \cdot 10^6$ cycles. During the fatigue test, there was a fracture through the aluminum alloy at the joint, very similar to PF failure mode.
 3. It should be expected that the REW joint would show significantly better mechanical characteristics than the RSW joint, if the joining was performed with aluminum of greater thickness (up to 6 mm). Moreover, it should be noted that the advantage of REW joint over RSW joint can be expected in terms of joining dissimilar materials that are not easily welded, such as the joint of steel and carbon materials or sandwich panels of small thickness, which will be the subject of further research.

Author Contributions: Conceptualization, A.Đ.; Investigation, A.Đ., D.M., Z.B., D.K., M.M. and B.M.; Resources, Z.B. and D.K.; Supervision, D.M.; Writing—original draft, A.Đ. and D.M.; Writing—review & editing, A.Đ., D.M., M.M., B.M. and V.K. All authors have read and agreed to the published version of the manuscript.

Funding: This research received no external funding.

Institutional Review Board Statement: Not applicable.

Informed Consent Statement: Not applicable.

Data Availability Statement: Not applicable.

Acknowledgments: The results presented in this paper were obtained through project “Research and analysis of advanced joining technology of dissimilar materials that are used in the development of lightweight structures” BI-BA/21-23-026 in the framework of the bilateral scientific cooperation between the Republic of Slovenia and Bosnia and Herzegovina. This research was financially supported by the Ministry of Education, Science and Technological Development of the Republic of Serbia (Contract No. 451-03-9/2021-14/200109).

Conflicts of Interest: The authors declare no conflict of interest.

References

1. Schmitt, J.H.; Lung, T. New developments of advanced high-strength steels for automotive applications. *Comptes. Rendus. Physique* **2018**, *19*, 641–656. [[CrossRef](#)]
2. Galán, J.; Samek, L.; Verleysen, P.; Verbeken, K.; Houbaert, Y. Advanced high strength steels for automotive industry. *Rev. Metal.* **2012**, *48*, 118–131. [[CrossRef](#)]
3. Bader, B.; Türck, E.; Vietor, T. Multi Material Design. A Current Overview of the Used Potential in Automotive Industries. In *Technologies for Economical and Functional Lightweight Design (Zukunftstechnologien für den MultiFunktionalen Leichtbau)*; Dröder, K., Vietor, T., Eds.; Springer: Berlin/Heidelberg, Germany, 2019.
4. Gerson, M.; Christopher, S.; Thomas, O. Process characteristics and load-bearing capacities of joints welded with elements for the application in multi-material design. *Weld. World* **2017**, *61*, 435–442.
5. Reiichi, S.; Chin, R. Dissimilar Metals Joining Process Using GMAW has High Strength and One side Access Characteristic, and the Automation Robot System. In *Proceedings of the 71ST IIW Annual Assembly 2018, Commission XII “Arc Welding Processes and Production Systems”, Bali, Indonesia, 16–18 July 2018.*

6. Aydin, H. The mechanical properties of dissimilar resistance spot-welded DP600–DP1000 steel joints for automotive applications. *J. Automob. Eng.* **2014**, *229*, 599–610. [[CrossRef](#)]
7. Reyes, G.; Gupta, S. Manufacturing and mechanical properties of thermoplastic hybrid laminates based on DP500 steel. *Compos. Part A Appl. Sci. Manuf.* **2009**, *40*, 176–183. [[CrossRef](#)]
8. Djuric, A.; Milčić, D.; Klobčar, D.; Marković, B. Multi-objective optimization of the resistance spot-welding process parameters for the welding of dual-phase steel DP500. *Mater. Technol.* **2021**, *2*, 201–206. [[CrossRef](#)]
9. Tisza, M.; Czinege, I. Comparative study of the application of steels and aluminium in lightweight production of automotive parts. *Int. J. Lightweight Mater. Manuf.* **2018**, *1*, 229–238. [[CrossRef](#)]
10. Wan, Z.; Wang, H.P.; Chen, N.; Wang, M.; Carlson, E.B. Characterization of intermetallic compound at the interfaces of Al-steel resistance spot welds. *J. Mater. Process. Technol.* **2017**, *242*, 12–23. [[CrossRef](#)]
11. Arghavani, M.R.; Movahedi, M.; Kokabi, A.H. Role of zinc layer in resistance spot welding of aluminium to steel. *Mater. Des.* **2016**, *102*, 106–114. [[CrossRef](#)]
12. Ibrahim, I.; Ito, R.; Kakiuchi, T.; Uematsu, Y.; Yun, K.; Matsuda, C. Fatigue behavior of Al/steel dissimilar resistance spot welds fabricated using Al–Mg interlayer. *Sci. Technol. Weld. Join.* **2016**, *21*, 223–233. [[CrossRef](#)]
13. Gullino, A.; Matteis, P.; D’Aiuto, F. Review of aluminium-to-steel welding technologies for car-body applications. *Metals* **2019**, *9*, 315. [[CrossRef](#)]
14. Pouranvari, M. Critical assessment: Dissimilar resistance spot welding of aluminium/steel: Challenges and opportunities. *Mater. Sci. Technol.* **2017**, *33*, 1705–1712. [[CrossRef](#)]
15. Mortazavi, S.N.; Marashi, P.; Pouranvari, M.; Masoumi, M. Investigation on joint strength of dissimilar resistance spot welds of aluminum alloy and low carbon steel. *Adv. Mater. Res.* **2011**, *264*, 384–389. [[CrossRef](#)]
16. Harish, M.R.; Jidong, K.; Liting, S.; David, R.S.; Blair, E.C. Effect of specimen configuration on fatigue properties of dissimilar aluminum to steel resistance spot welds. *Int. J. Fatigue* **2018**, *116*, 13–21.
17. Shi, L.; Kang, J.; Shalchi-Amirkhiz, B.; Sigler, D.R.; Haselhuhn, A.S.; Carlson, B.E. Effect of coating type on microstructure and mechanical behavior of resistance spot welds of thin X626 aluminum sheet to low carbon steel. *J. Mater. Process. Technol.* **2019**, *264*, 438–447. [[CrossRef](#)]
18. Jidong, K.; Harish, M.R.; David, R.S.; Blair, E.C. Tensile and fatigue behaviour of AA6022-T4 to IF steel resistance spot welds. *Procedia Struct. Integr.* **2017**, *5*, 1425–1432.
19. Zhang, X.; Yao, F.; Ren, Z.; Yu, H. Effect of welding current on weld formation, microstructure, and mechanical properties in resistance spot welding of CR590T/340Y galvanized dual phase steel. *Materials* **2018**, *11*, 2310. [[CrossRef](#)]
20. Anijdan, S.H.; Sabzi, M.; Ghobeiti-Hasab, M.; Roshan-Ghiyas, A. Optimization of spot welding process parameters in dissimilar joint of dual phase steel DP600 and AISI 304 stainless steel to achieve the highest level of shear-tensile strength. *Mater. Sci. Eng. A* **2018**, *726*, 120–125. [[CrossRef](#)]
21. Ordoñez, J.H.; Ambriz, R.R.; García, C.; Plascencia, G.; Jaramillo, D. Overloading effect on the fatigue strength in resistance spot welding joints of a DP980 steel. *Int. J. Fatigue* **2019**, *121*, 163–171. [[CrossRef](#)]
22. Hongqiang, Z.; Xiaoming, Q.; Yang, B.; Fei, X.; Haiyan, Y.; Yanan, S. Resistance spot welding macro characteristics of the dissimilar thickness dual phase steels. *Mater. Des.* **2014**, *63*, 151–158.
23. Shi, L.; Kang, J.; Gesing, M.; Chen, X.; Haselhuhn, A.S.; Carlson, B.E. Effect of notch root angle on fatigue behavior of aluminum to steel resistance spot welds. *Int. J. Fatigue* **2020**, *141*, 105866. [[CrossRef](#)]
24. Arnold. Brochure Flexweld®Resistance Element Welding. 2020. Available online: <https://www.arnold-fastening.com/en/products/resistance-element-welding/flexweld> (accessed on 25 February 2021).
25. Ling, Z.; Li, Y.; Luo, Z.; Feng, Y.; Wang, Z. Resistance element welding of 6061 aluminum alloy to uncoated 22MnMoB boron steel. *Mater. Manuf. Processes* **2016**, *31*, 2174–2180. [[CrossRef](#)]
26. Ling, Z.; Li, Y.; Luo, Z.; Ao, S.; Yin, Z.; Gu, Y.; Chen, Q. Microstructure and fatigue behavior of resistance element welded dissimilar joints of DP780 dual-phase steel to 6061-T6 aluminium alloy. *Int. J. Adv. Manuf. Technol.* **2017**, *92*, 1923–1931. [[CrossRef](#)]
27. Qiu, R.; Wang, N.; Shi, H.; Cui, L.; Hou, L.; Zhang, K. Joining steel to aluminum alloy by resistance spot welding with a rivet. *Int. J. Mater. Res.* **2015**, *106*, 60–64. [[CrossRef](#)]
28. Daniel, H.; Fan, Z.; Xiangfan, F. Fatigue strength of rivet resistance spot welding technique in comparison with self-piercing riveting for multi-material body-in-white structure. *J. Mater. Eng. Perform.* **2021**, *30*, 3806–3821.
29. Sizhe, N.; Yunwu, M.; Ming, L.; Chaoqun, Z.; Yongbing, L. Joint formation mechanism and performance of resistance rivet welding (RRW) for aluminum alloy and press hardened steel. *J. Mater. Process. Technol.* **2020**, *286*, 116830.
30. Troschitz, J.; Vorderbrüggen, J.; Kupfer, R.; Gude, M.; Meschut, G. Joining of thermoplastic composites with metals using resistance element welding. *Appl. Sci.* **2020**, *10*, 7251. [[CrossRef](#)]
31. Manladan, S.M.; Zhang, Y.; Ramesh, S.; Cai, Y.; Ao, S.; Luo, Z. Resistance element welding of magnesium alloy and austenitic stainless steel in three-sheet configurations. *J. Mater. Process. Technol.* **2019**, *274*, 116292. [[CrossRef](#)]
32. Manladan, S.; Yusof, F.; Ramesh, S.; Zhang, Y.; Luo, Z.; Ling, Z. Resistance Element Welding of Magnesium Alloy/austenitic Stainless Steel. In *IOP Conference Series: Materials Science and Engineering*; IOP Publishing: Bristol, UK, 2017; p. 238.

33. Pouranvari, M.; Sobhani, S.; Goodarzi, F. Resistance spot welding of MS1200 martensitic advanced high strength steel: Microstructure-properties relationship. *J. Manuf. Process.* **2018**, *31*, 867–874. [[CrossRef](#)]
34. Manladan, S.M.; Yusof, F.; Ramesh, S.; Fadzil, M.; Luo, Z.; Ao, S. A review on resistance spot welding of aluminum alloys. *Int. J. Adv. Manuf. Technol.* **2017**, *90*, 605–634. [[CrossRef](#)]
35. Pouranvari, M.; Marashi, S.P.H.; Mousavizadeh, S.M. Dissimilar resistance spot welding of DP600 dual phase and AISI 1008 low carbon steels: Correlation between weld microstructure and mechanical properties. *Ironmak. Steelmak.* **2011**, *38*, 471–480. [[CrossRef](#)]